Persistent-Current Magnetization of Nb_3Sn Strands: Influence of Applied Field Angle and Transport Current

X. Xu, M. Majoros, M. D. Sumption and E. W. Collings

***Abstract*—For many accelerator magnets field quality at the bore is a critical requirement for which reason it is necessary to fully characterize the persistent-current magnetization of strands of the kind under consideration for these magnets. The magnetization of a strand is generally measured in a magnetometer. However, certain effects can differentiate such measurements from the true magnetizations of strands in magnets. This report focuses on persistent-current magnetization: (i) measured by vibrating-sample magnetometer on segments of strand extracted from a section of heat treated Nb_3Sn cable as functions of angle of the applied field and (ii) calculated as function of applied transport current. It is found that the magnetization of a strand in a cable increases by ~10% as the field applied to the cable is shifted from edge-on to face-on, and that the difference between the current-on and current-off magnetizations is not significant until close to the operational field of a magnet.**

***Index Terms*—angular dependence; persistent-current magnetization; magnetization and transport current; Nb_3Sn strands.**

I. Introduction

THE PRESENT superconducting magnets of the large hadron collider (LHC) are all wound with Nb-Ti Rutherford cables. Contributing to the LHC's success are what might be termed the qualities of the dipole and quadrupole fields, great care having been taken to control the parasitic magnetizations (coupling- and persistent-current) present in the magnet windings and other magnetic effects. The magnetic properties and field qualities of the LHC's present Nb-Ti magnets provide bench-marks against which those of any future magnets can be compared. A series of upgrades to the LHC are planned the immediate ones requiring magnets wound with Nb_3Sn cables: (1) Additional beam collimators are to be installed in the dispersion-suppressor (DS) segments of the ring, to make room for which it is proposed to replace pairs of 8.33 T, 15 m, Nb-Ti dipoles with pairs of 11 T, 11 m, Nb_3Sn dipoles [1]. The new magnets will need to be fully compatible (dimensions, field harmonic content, *etc.*) with the Nb-Ti magnets they are to replace [1], [2]. Particular attention will need to be given to differences in parasitic magnetization. (2) The LHC's high luminosity upgrade (High Lumi) calls for the installation by 2022-2023 of sixteen low-β quadrupole magnets, peak field 13 T also to be wound with Nb_3Sn cable [2]-[4]. In support of High Lumi the US Accelerator Research Program (LARP) has been developing a series of Nb_3Sn-wound test quadrupoles designated TQ, LQ, and HQ [3], [4]. As a contribution to this development program the present group (including OSU's Center for Superconducting and Magnet Materials, CSMM) has studied the properties of TQ-class 27-strand Rutherford cables [5] and more recently the magnetic properties of strand and cable for the HQ quadrupole.

An increasing field applied to a superconducting strand is shielded by a so-called persistent current equivalent to a Bean-type magnetization, M_{sh} (one half of the full height of a magnetization loop). This leads to a ramp-rate-independent cable magnetization given by $M_{sh} = (2/3\pi)\lambda_s\lambda_c J_c d_{eff}$ in which λ_s and λ_c are the strand- and cable fill factors, respectively, J_c is the critical current density, and d_{eff} is the strand's effective subelement diameter. The large d_{eff}s of Nb_3Sn strands (typically 10 times larger than those of Nb-Ti strands) combined with high J_c, leads to very high M_{sh}, making careful studies of this necessary. Usually we measure magnetization with the applied field perpendicular to the strand axis. However, in an accelerator magnet the angle between the magnetic field and the broad face of a Rutherford cable may vary from 90° (face-on) to 0° (edge-on) [6]. Correspondingly, the angle between the magnetic field and an individual strand in the cable varies (in the case of the HQ cable [6]-[8], for example) from 90 to 73°, since the angle between the strand axis and the cable axis is $\tan^{-1}$(width/half-lay-pitch) = 17°. To determine the persistent-current magnetization contributed by all the strands in a magnet, it is necessary to measure the variation of strand magnetization with applied-field angle from 90 to 73°; for completeness, angular dependence from 0 to 90° was measured.

Also, strand magnetization is generally measured in the absence of transport current. To render the results relevant to magnet-cable magnetization the effect of transport current, I, should be considered. The first to do so was LeBlanc [9] whose analytical calculation showed the magnetization changing according to $M/M_0=1-(I/I_c)^2$ where I and I_c (the critical current) are to be evaluated at the particular fields of interest as in [7]. LeBlanc modelled a semi-infinite slab of

Manuscript received August 12th, 2014. This work was supported in part by the U.S. Dept. of Energy, Office of High Energy Physics, under Grants No. DE-FG02-95ER40900 (OSU) and a DOE SBIR.

X. Xu, M. Majoros, M. Sumption and E. Collings are with the Ohio State University, Columbus, Ohio 43202 USA (X. Xu phone: 515-441-3429; e-mail: xu.452@osu.edu).

TABLE I.
SPECIFICATIONS OF THE STRAND USED IN THE MEASUREMENTS OF FIELD ANGLE DEPENDENCE OF MAGNETIZATION

STRAND DETAILS	
Cable name	HQ1021ZB (LBNL)
Cable packing factor, %	85.53
Strand count in cable	35
Strand diameter, mm	0.778
No. of subelements	108/127
Effective subelement diameter, μm	61.3
Non-Cu content, %	44.9
Heat treatment	210°C/72h+400°C/48h+ 650°C/48h

superconductor; a cylindrical or tubular superconductor is expected to yield a different relationship. Cross and Goldfarb [10] investigated this experimentally by measuring the magnetization of a current-carrying Nb-Ti strand using a Hall probe magnetometer. In this work we continue the study of the transport current effect on magnetization both by finite element modelling (FEM) and analytically [11], [12].

II. FIELD ANGLE DEPENDENCE OF MAGNETIZATION

A. Strands and measurements

Measurements of magnetization as function of the angle, θ, between the magnetic field and the strand axis were made on a sample of strand extracted from a segment of Nb_3Sn Rutherford cable wound and treated at the Lawrence Berkeley National Laboratory (LBNL). The details of the cable (LBNL Code HQ1021ZB) and strand are given in Table I and more detailed information can be found elsewhere [7]. The 4 mm long sample was mounted on a quartz holder in preparation for measurement using the vibrating sample magnetometer (VSM) accessory to Quantum Design Model 6000 PPMS system. Magnetization vs. magnetic field (*M-B*) loops were measured at 4.5 K and 1.9 K with a sweep rate of 13 mT/s for θ values of 0, 30, 45, 60, 70, 75, 80, and 90°. The magnetization was obtained by dividing the measured moment by the whole sample volume. The overall error is estimated to be less than 5%.

B. Analytical Model

Let the internal-Sn Nb_3Sn subelement be represented by a hollow cylinder of uniform, isotropic superconductor. Then as

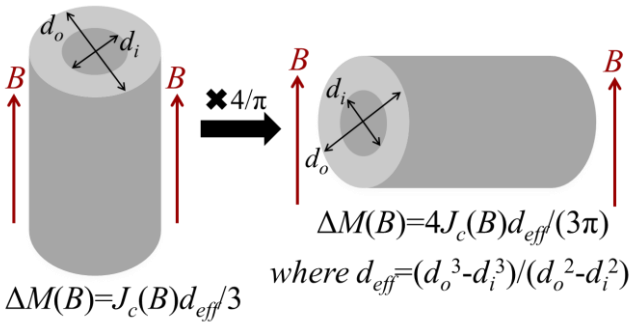

Fig. 1. The magnetizations of a uniform, isotropic superconductor subelement in a parallel field and a perpendicular field, both in fully penetrated state.

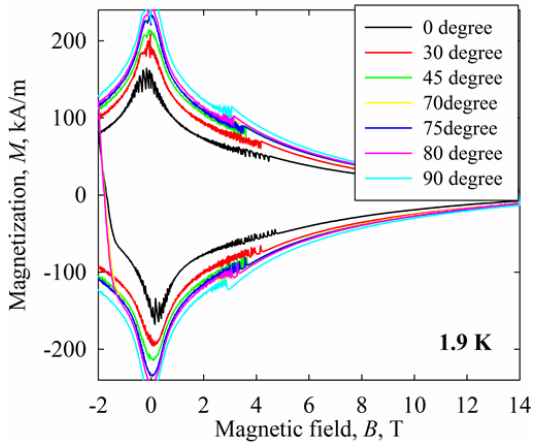

Fig. 2. The *M-B* loops of HQ1021ZB at 1.9 K for various angles.

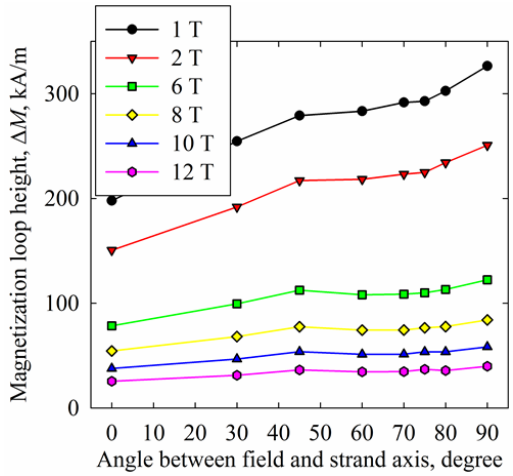

Fig. 3. The variations of ΔM against θ for different fields at 1.9 K.

illustrated in Fig. 1, when the applied field direction is shifted from parallel to perpendicular, the heights of *M-B* loops, ΔM, according to the "semi-Bean" model (*i.e.*, assuming the critical current density J_c is the same everywhere in the superconductor) increases by $4/\pi = 27\%$ in the fully penetrated state. Calculation to predict the variation of subelement ΔM with θ is difficult, more so for the full strand with its plurality of twisted subelements which are neither uniform (*e.g.*, due to Sn concentration gradient across the Nb_3Sn layer) nor ideally isotropic (*e.g.*, the Nb_3Sn grains are not perfectly equiaxed). For these reasons $\Delta M(\theta)$ was explored experimentally.

C. Results

The 1.9 K *M-B* loops are displayed in Fig. 2. The extracted ΔMs at selected fields plotted as function of θ were found to increase by 54~56% as θ shifted from 0 to 90° (Fig. 3), twice as great as the expected 27%. It is likely that the above-mentioned difficulties contributed to this difference. The increase in $\Delta M(\theta)$ from θ~73° to θ =90°, corresponding to a change in orientation of an applied field to a Rutherford cable from "edge-on" to "face-on" is around 10%.

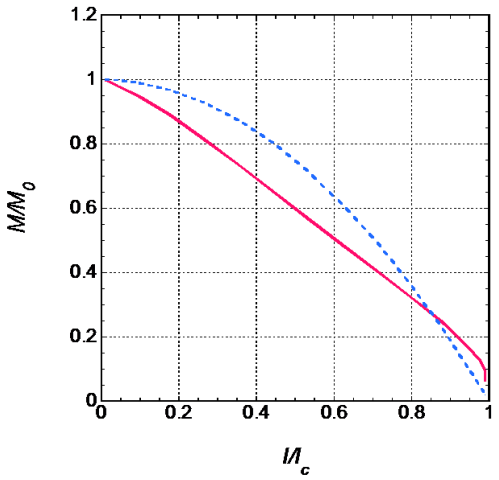

Fig. 4. A comparison of the effect of transport current on the magnetizations of a slab superconductor based on LeBlanc's model (the blue dashed curve) and on a cylindrical superconductor based on our modeling (the red solid curve).

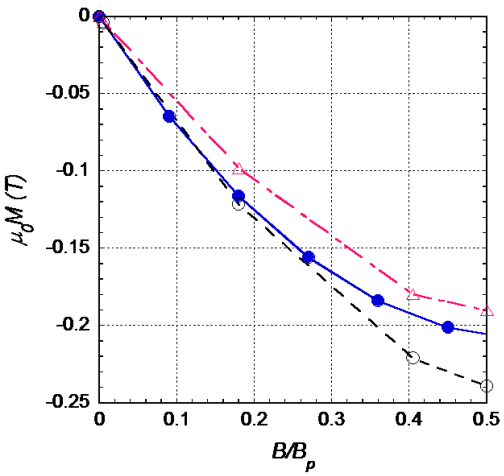

Fig. 6. A comparison of magnetizations of case 1 (the transport current was first ramped up to $0.5I_c$ and then magnetic field was ramped up to $0.5B_p$, black open circle), case 2 (the applied field was ramped up to $0.5B_p$ with no transport current, red open triangle) and case 3 (a simultaneous application of transport current up to I_c and applied field up to B_p, blue solid circle).

III. Transport Current Dependence of Magnetization

A. The effect of sample shape

As mentioned above, LeBlanc calculated the effect of transport current on the magnetization of a semi-infinite slab of superconductor [9] and showed M/M_0 (the ratio of current-on to current-off magnetizations) varied with normalized current, I/I_c, according to

$$\frac{M}{M_0} = 1 - \left(\frac{I}{I_c}\right)^2 \quad (1)$$

It is expected that a tubular or cylindrical object would yield a different relationship. To explore this possibility we modelled a cylindrical superconducting wire with radius of 1 mm, critical current density $J_c = 1\times10^9$ A/m^2 (1 μV/cm criterion, independent of B), and power-law current-voltage (I-V) curve with an n-value of 25. Following [9] we first applied the magnetic field to above the penetration field, B_p, and then applied the transport current up to $0.99I_c$. The cylindrical- and the previous slab results are compared in Fig. 4.

B. The effect of current/field sequence

In the above studies the field was first applied to its final value and then the current was turned on. In what follows we explore two other sequences including a zero-current "control". We refer to them as: (i) Case-1: A transport current of $0.5I_c$ is turned on and then an applied field is ramped up to $0.5B_p$. (ii) Case-2: In the absence of transport current the applied field is ramped up to $0.5B_p$; only the persistent current is present. (iii) Case-3: The transport current and the applied field are simultaneously ramped up to I_c and B_p, respectively. The current distributions of the three cases as B reached ~$0.4B_p$ are shown in Fig. 5 and the calculated $M(B)$ curves are presented in Fig. 6.

In determining M/M_0 for a magnet it is necessary to express the RHS of Equation (1) in terms of the B (produced by the current I) along with the I_c corresponding to that field. This can be done on a point-by-point basis as in [7] wherein M/M_0 was obtained for some low (injection) and high (operation) accelerator magnet fields. But more useful is an analytical relationship. This can be formed by recognizing that I lies on the magnet load line ($I = kB$, where k is the magnet constant) and that I_c at the corresponding B is given by a suitable pinning-related function. Our analysis begins by extending the load line, $I = kB$, to intersect the short-sample $I_c(B)$ at a point (I_{max}, B_{max}) and by selecting for $I_c(B)$ the Kramer-Dew-Hughes relationship $I_c = I_0(1-b)^2/\sqrt{b}$ in which $b = B/B_{irr}$ where B_{irr} is

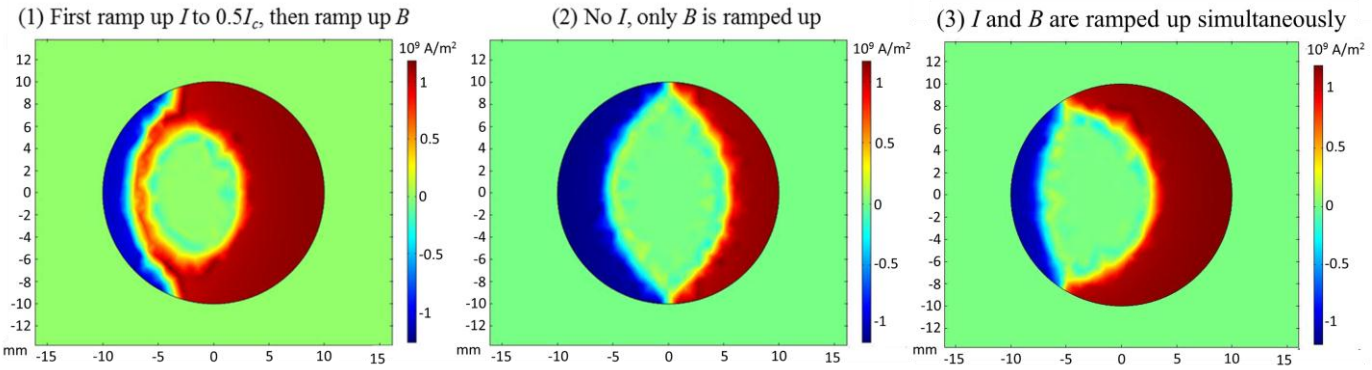

Fig. 5. Current distributions as B reaches ~$0.4B_p$ for Case-1 (the transport current was ramped up to $0.5I_c$ before the magnetic field was ramped up), Case-2 (the applied field was ramped up with no transport current) and Case-3 (a simultaneous ramp up of transport current and applied field).

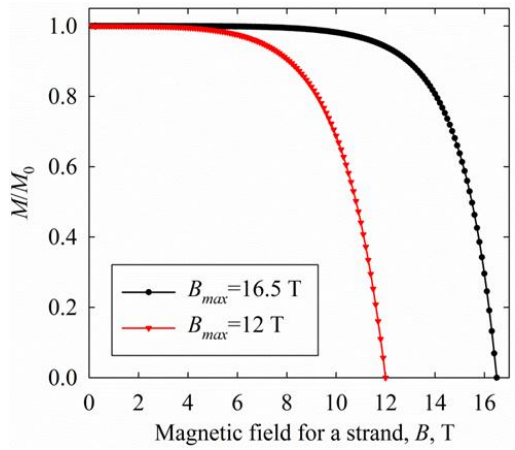

Fig. 7. The change of magnetization with B for B_{max}=16.5 T and 12 T, respectively. The calculation was based on LeBlanc's model.

the irreversibility field. Thus at some arbitrary field, B:

$$I = kB, \qquad and \qquad I_c = I_0 (1-b)^2 / \sqrt{b} \tag{2}$$

and at the intersection point, whereat $b_{max} = B_{max}/B_{irr}$:

$$I_{\max} = kB_{\max}, \qquad and \qquad I_{\max} = I_0 (1-b_{\max})^2 / \sqrt{b_{\max}} \tag{3}$$

Then it follows that LeBlanc's Equation (1) can be expressed as:

$$\frac{M}{M_0} = 1-\left(\frac{I}{I_c}\right)^2 = 1-\left(\frac{B}{B_{\max}}\right)^3 \left(\frac{B_{irr}-B_{\max}}{B_{irr}-B}\right)^4 \tag{4}$$

In the magnet itself, although all the strands carry the same current, they are in different fields. Thus, there are a band of load lines (defined by $I_{max} = kB_{max}$) for the strands. Equation (4) applies to each strand with its own B, B_{max}, I_{max} values.

To associate this result with the magnetization of an accelerator cable we assume B_{max} values of 12 T and 16.5 T (corresponding to two difference magnet strand lines) and a B_{irr} of 24 T for the Nb_3Sn strand with which it is wound. After inserting these data, Equation (4) enables M/M_0 to be plotted versus B as in Fig. 7.

From Fig. 7 we can see that for B_{max}=16.5 T the difference between M and M_0 won't reach 1% until B reaches 9 T. This indicates that transport current mainly suppresses magnetization at high fields (those close to operation field). Equation (4) indicates how transport current influences the magnetizations of strands in a magnet based on LeBlanc's model. We are developing a more accurate model for practical Nb_3Sn strands, considering both the shape effect and the $I_c(B)$ relationship. An experiment to measure the magnetization change with transport current using Hall probes is also being set up.

IV. Concluding Summary

When the field applied to a Rutherford cable is shifted from face-on to edge-on, the orientation of the field with respect to the stand axis shifts from 90° (FO) to $\tan^{-1}$(width/half-lay-pitch) = 17° for the HQ cable. Accordingly it was of interest to measure the strand's ΔM as function of applied field angle, θ, from zero degrees (parallel to the axis) to 90°. The observed increase from the cable-relevant angles of ~73° to 90° was in the range of 10% - not a large effect. The persistent-current magnetization of a cable in a magnet is expected to be decreased by the presence of increasing transport current, an effect initially calculated for a semi-infinite slab by LeBlanc. In studying this effect further it was found (by FEM calculation) that a sample's shape-change from slab to cylinder resulted in a significant change in the slope of the M/M_0 versus I/I_c curve. Also as computed by FEM the transport effect differed in response to the order in which currents and fields were applied to a sample in the pre-penetration state ($b = B/B_p < 1$). The negative slope of M versus B increased in the sequence: (current first then field) < (simultaneous current and field) at an average rate, dM/db, of -0.5 T. The report concludes with an analytic extension of the LeBlanc relationship $M/M_0 = 1 - (I/I_c)^2$ in the form of an M/M_0 versus B, useful for magnet applications. In this expression, the influence of magnet load-line change can be predicted simply by changing the value of B_{max}, *e.g.* from 12 T to 16.5 T. In the latter case it was found that the difference between the current-on and current-off magnetizations (M and M_0) does not reach even 1% until B reaches 9 T. The report is a case study of some magnetic- and transport-related properties of Nb_3Sn strands and provides a starting point for future work on other magnet-relevant strands such as Bi:2212 and YBCO coated conductor tapes whose like properties may turn out to vary much more strongly.

Acknowledgment

We thank LBNL for supplying the cables for this study.

References

[1] M. Karppinen, N. Andreev, G. Apollinari, *et al.*, "Design of 11 T twin-aperture dipole demonstrator magnet for LHC upgrades", *IEEE Trans. Appl. Supercond.*, vol. 22, Issue 3, Pages 4901504, June 2012; see also M. Karppinen, "11 T dipole status May 2012", https://espace.cern.ch/dsdipole/-; see also: hilumilhc.web.cern.ch/hilumilhc/activities/11-T/WP11/

[2] L. Bottura, G. de Rijk, L. Rossi, and E. Todesco, "Advanced accelerator magnets for upgrading the LHC", *IEEE Trans. Appl. Supercond.*, vol. 22, Issue 3, June 2012, Art. No. 40002008.

[3] H. Felice, S. Caspi, P. Ferracin, V. Kashikin, *et al.*, "Magnetic and mechanical analysis of the HQ model quadrupole designs for LARP", *IEEE Trans. Appl. Supercond.*, vol. 18, Issue 2, Pages 281-284, June 2008.

[4] S. Caspi, G. Ambrosio, M. Anerella, E. Barzi, *et al.*, "Design of a 120 mm bore 15 T quadrupole for the LHC upgrade phase II", *IEEE Trans. Appl. Supercond.*, vol. 20, Issue 3, Pages 144-147, June 2010.

[5] E.W. Collings, M.D. Sumption, M.A. Susner, D.R. Dietderich, E. Barzi, A.V. Zlobin, Y. Ilyin, and A. Nijhuis, "Influence of a stainless steel core on coupling loss, interstrand contact resistance, and magnetization of an Nb_3Sn Rutherford cable", *IEEE Trans. Appl. Supercond.*, vol. 21, Issue 3, Pages 2367-2371, June 2011.

[6] X. Wang, G. Ambrosio, F. Borgnolutti, M. Buehler *et al.*, "Multipoles induced by inter-strand coupling currents in LARP Nb_3Sn quadrupoles", *IEEE Trans. Appl. Supercond.*, vol. 24, Issue 3, June 2014, Art. No. 4002607.

[7] E. W. Collings, M. A. Susner, M. D. Sumption, and D. R. Dietderich, "Extracted strand magnetizations of an HQ type Nb_3Sn Rutherford cable and estimation of transport corrections at operating and injection fields", *IEEE Trans. Appl. Supercond.*, vol. 24, Issue 3, June 2014, Art. No. 4802605.

[8] E. W. Collings, M. D. Sumption, M. A. Susner, D. R. Dietderich, E. Kroopshoop, and A. Nijhuis, "Coupling- and persistent-current magnetizations of Nb_3Sn Rutherford cables with cores of stainless steel

and woven glass-fiber tape measured by pick-up coil magnetometry", *IEEE Trans. Appl. Supercond.*, vol. 23, Issue 3, June 2013, Art. No. 4702305.

[9] M. A. R. LeBlanc, "Influence of transport current on magnetization of a hard superconductor", *Phys. Rev. Lett.*, vol. 11, Issue 4, Pages 149-152, Aug 1963.

[10] R. W. Cross and R. B. Goldfarb, "Hall probe magnetometer for SSC magnet cables - effect of transport current on magnetization and flux creep", *IEEE Trans. Magn.*, vol. 27, Issue 2, Pages 1796-1798, March 1991.

[11] Z. Hong, A. M. Campbell and T. A. Coombs, "Numerical solution of critical state in superconductivity by finite element software", *Supercond. Sci. Tech.*, vol. 19, Issue 12, Pages 1246-1252, Oct. 2006.

[12] Z. Hong, L. Ye, M. Majoros, A. M. Campbell and T. A. Coombs, "Numerical estimation of AC loss in MgB_2 wires in self-field condition", *J. Supercond. Nov. Magn.*, vol. 21, Issue 3, Pages 205-211, June 2008.